Imaging Plasmonic Fields with Atomic Spatiotemporal Resolution

Jianxiong Li, Erfan Saydanzad, and Uwe Thumm

Phys. Rev. Lett. **120**, 223903 — Published 1 June 2018

DOI: 10.1103/PhysRevLett.120.223903

Imaging plasmonic fields with atomic spatiotemporal resolution

Jianxiong Li, Erfan Saydanzad, and Uwe Thumm
Department of Physics, Kansas State University, Manhattan, Kansas 66506, USA
(Dated: April 25, 2018)

We propose a scheme for the reconstruction of plasmomic near-fields at isolated nanoparticles from infrared-streaked extreme-ultraviolett photoemission spectra. Based on quantum-mechanically modeled spectra, we demonstrate and analyze the accurate imaging of the IR-streaking-pulse-induced transient plasmonic fields at the surface of gold nanospheres and nanoshells with sub-femtosecond temporal and sub-nanometer spatial resolution.

PACS numbers:

The dynamical response of atoms, molecules, and solids to electromagnetic radiation is governed by electronic processes that occur at the timescale of one atomic time unit (24 attoseconds = 24 as = 24×10^{-18} s) [1]. Driven by rapid progress in the development of table-top attosecond-duration light sources over the past two decades [2–6], this timescale has become accessible in ultrafast laser laboratories. This enables the recording of streaked photoelectron spectra [7–14] and two-photon-two-pathway-photoemission interferograms [5, 6, 15–17] by employing intense few-optical-cycle infrared (IR) laser pulses in combination with phase-synchronized delayed isolated attosecond extreme ultraviolet (XUV) pulses or pulse trains, respectively, by measuring photoelectron yields as functions of the adjustable delay τ between the IR and XUV pulse or pulse train. As this technique is being further refined, emerging attosecond time-, spin-, energy-, and emission-angle-resolved photoelectron spectroscopy is starting to allow, e.g., the imaging of ultrafast bandstructure changes, dynamical screening effects in solids, and electronic correlation in magnetic materials [6, 16, 17].

Recent extensions of attosecond time-resolved spectroscopy to solid surfaces [5, 6, 9, 11, 14–16, 18] and nanoparticles [13] hold promise to enable the study of transient collective electronic processes in solids with unprecedented temporal and added nanometer-scale (1 nm = 10^{-9} m) spatial resolution. Such investigations are of applied interest, e.g., for the development of ultrafast electro-optical switches and computing hardware based on layered nanostructures [3, 19] and novel attosecond nanoplasmonic-field-imaging techniques [20–24]. They are further propelled by advances in nanotechnology allowing the controlled assembly of metallic structures that are two orders of magnitude smaller than the wavelength of (visible) light and, near their plasmon-resonance frequency, respond very strongly to incident IR and visible electric fields that coherently drive a macroscopic number of conduction electrons, leading to electric-near-field-intensity enhancements of up to 10^4 [25–27]. Such extremely enhanced plasmonic fields are the key physical phenomenon behind emerging research efforts in nanoplasmonically enhanced photocatalysis [28] and light harvesting [29], light–triggered drug release from nanoparticles [30, 31], and electron-point-source development [32].

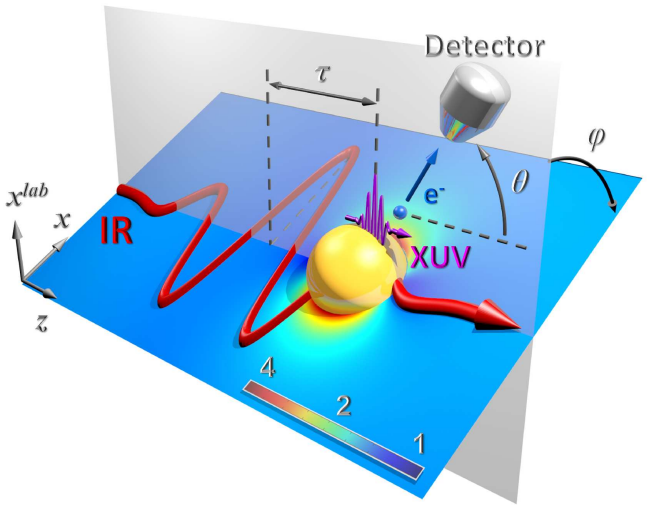

FIG. 1: (Color online) Schematic of attosecond nanoplasmonic imaging. An attosecond XUV pulse emits electrons into the field of a delayed IR streaking laser pulse, whose polarization direction can be rotated by a variable angle φ relative to the XUV-pulse polarization. The linear color/gray scale represents the electric-field-strength enhancement for 50 nm radius Au nanospheres in 720 nm incident IR pulses.

The detailed analysis of spatiotemporally-resolved photoemission experiments at the sub-fs and nm scales and the exploration of novel nanoplasmonic applications rely on discipline-transcending numerical modeling within the emerging field of quantum plasmonics [8, 19, 25, 27, 33–35]. In this Letter we suggest a scheme for the reconstruction of plasmonic near-fields of isolated nanoparticles from IR-streaked XUV photoemission spectra with sub-fs temporal and nm spatial resolution. We analyze the accuracy of this imaging scheme for quantum-mechanically modeled streaked spectra from Au nanospheres [33, 34] (Fig. 1), demonstrating excellent agreement with plasmonic near-fields obtained within classical Mie theory [36].

We study the photoemission from the conduction band of Au nanospheres of radius $R = 50$ nm by isolated Gaus-

sian attosecond XUV pulses

$$\mathbf{E}_X(\mathbf{r},t) = \hat{\mathbf{x}}^{lab} E_X \exp\left[-2\ln 2\Big(\frac{t-t_z}{\tau_X}\Big)^2 \right] e^{-i\omega_X(t-t_z)} \tag{1}$$

with central photon energy $\omega_X = 50$ eV, full width at half intensity maximum (FWHIM) $\tau_X = 200$ as, retardation $t_z = z/c$, and vector potential $\mathbf{A}_X(\mathbf{r},t) = \int_t^\infty dt'\, \mathbf{E}_X(\mathbf{r},t')$ into the electric field of delayed 720 nm, 2.47 fs (FWHIM), and 10^{11} W/cm^2 (spheres) or 10^{10} W/cm^2 (shells) peak intensity streaking pulses. Atomic units are used throughout this work, unless specified otherwise. Both pulses propagate along the z-axis of the laboratory-fixed $x^{lab}yz$ coordinate system that is centered in the nanosphere. The XUV and IR pulse are linearly polarized along the x^{lab}- and x-axis, respectively, with adjustable relative polarization direction φ (Fig. 1). Their time delay τ is assumed positive if the XUV pulse precedes the IR pulse. Photoelectrons are detected in the $x^{lab}z$-plane under the angle θ with respect to the z-axis, i.e., in direction $\hat{\mathbf{n}} = (\theta, \varphi)$.

The large streaking pulse wavelength compared to the size of the nanosphere implies *'quasi-static' conditions* for which Mie calculations show the net IR field to be efficiently screened inside and oriented perpendicular to the metallic nanoparticle surface, as for static external fields [36, 37]. For the assumed XUV and IR pulse parameters, photoelectrons are exposed to the streaking field over less than 10 nm. Since the field strength of the IR-pulse-induced nanoplasmonic field decays outside the particle as $\sim (R/r)^3$, the spatial range of the enhancement is $\sim R$ [38]. The streaking pulse length is therefore short compared to the time it takes photoelectrons to escape the plasmonic near-field. The *'slow-escape condition'* [39] is thus met, under which photoelectrons do not experience the spatial variation of the streaking field after being emitted from nanoparticle surface.

We calculate the quantum-mechanical transition amplitude

$$T_i(\mathbf{k}_f,\tau) = i\int dt \int d\mathbf{r} \Psi^{\tau *}_{\mathbf{k}_f}(\mathbf{r},t)\mathbf{A}_X(\mathbf{r},t)\cdot\hat{\mathbf{p}}\Psi_i(\mathbf{r},t), \tag{2}$$

for photoemission by a single XUV photon from an initial state Ψ_i into the final state $\Psi^\tau_{\mathbf{k}_f}$ as a function of the final photoelectron momentum $\mathbf{k}_f$ and time delay τ within the velocity gauge and in single-active-electron approximation [33, 34]. $\hat{\mathbf{p}} = -i\nabla$ designates the electron momentum operator. We model initial conduction-band states,

$$\Psi_i(\mathbf{r},t) = \Psi_i(\mathbf{r})e^{-i\omega_i t}, \tag{3}$$

as bound states below the Fermi level of a spherical square well of radius $R = 50$ nm, whose depth $V_0 = -W_f - \sigma_c = -13.1$ eV is given by the work function $W_f = 5.1$ eV and conduction-band width $\sigma_c = 8$ eV [33].

In contrast to atomic targets, where the inhomogeneity of the streaking field can be neglected [8], for 100 nm diameter nanospheres the emitted electron is streaked by the *inhomogeneous* field $\mathbf{E}_{tot}(\mathbf{r},t)$, which we compute within Mie theory [36, 37] as superposition of the incident streaking pulse and its induced plasmonic response field. This allows us to represent the final photoelectron state as the exponentially damped generalized 'Volkov' wave function [33, 34]

$$\Psi^\tau_{\mathbf{k}_f}(\mathbf{r},t) = \frac{1}{\sqrt{2\pi}} f[l(\mathbf{r});\kappa] e^{i\mathbf{k}_f\cdot\mathbf{r}} e^{i\phi^\tau_{\mathbf{k}_f}(\mathbf{r},t)}, \tag{4}$$

with the position-dependent phase

$$\phi^\tau_{\mathbf{k}_f}(\mathbf{r},t) = \int_t^\infty dt' \mathbf{p}^2(\mathbf{r},t';\tau)/2. \tag{5}$$

The damping factor $f(l;\kappa) = exp[-l/(2\kappa)]$ accounts for photoelectrons that are excited ('born') by the XUV pulse at position $\mathbf{r}$ and scattered inside the nanosphere, without being detected. It depends on the photoelectron path length $l(\mathbf{r})$ inside the nanosphere, and the mean free path $\kappa = 5$ Å, which is approximately independent of the photoelectron kinetic energy within the energy range studied in this work [40]. We approximate $\Psi^\tau_{\mathbf{k}_f}$ semiclassically by calculating the initial momenta of electrons released at $\tilde{\mathbf{r}}_\tau(t) = \mathbf{r}$ at time t

$$\mathbf{p}(\mathbf{r},t;\tau) = \mathbf{k}_f + \int_t^\infty dt'\, \mathbf{E}_{tot}[\tilde{\mathbf{r}}_\tau(t'), t'+\tau]. \tag{6}$$

along classical photoelectron trajectories $\tilde{\mathbf{r}}_\tau(t')$ [10]. The photoemission probability as a function of photoelectron kinetic energy $\mathcal{E}_f$, time delay τ, and detection direction $\hat{\mathbf{n}}$ is obtained as an incoherent sum over all occupied initial states,

$$P(\mathcal{E}_f)\big|_{\tau,\hat{\mathbf{n}}} = \frac{1}{\sqrt{2\mathcal{E}_f}} \sum_{i\in occ} |T_i(k_f\hat{\mathbf{n}},\tau)|^2. \tag{7}$$

Figure 2 shows streaked photoelectron spectra for various detection angles (θ,φ). For a given relative polarization direction φ, the detected peak photoemission yield is largest along the XUV polarization direction ($\theta = 90°$) and decreases proportional to $\cos^2(\theta - 90°)$, following a dipole-emission pattern [Figs. 2(a)-2(c)]. The streaking-oscillation amplitude also reaches its maximum at $\theta = 90°$, due to emission across the maximally enhanced plasmonic near-field (Fig. 1). For the same detection angle θ, streaking oscillations for emission in forward $\varphi = 0°$ and backward $\varphi = 180°$ direction have opposite phase due to the dipole character of the induced plasmonic field [Figs. 2(d)-2(f)]. Streaking traces calculated according to Eqs. (2)-(7) follow the instantaneous net electric IR field $\mathbf{E}_{tot}$, in the same way as streaked spectra from atoms [7, 8] and surfaces [11, 12], retracing the instantaneous electric field strength of the incident streaking pulse.

The reconstruction of the net electric field $\mathbf{E}_{tot}$ at the nanoparticle surface constitutes a challenging inversion

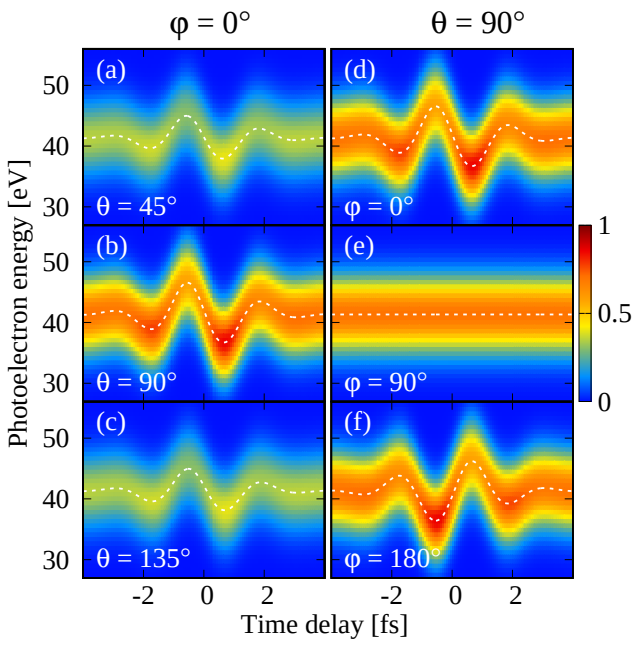

FIG. 2: (Color online) Streaked photoelectron spectra for 50 nm radius Au nanospheres at detection angles (a)-(c) $\varphi = 0^\circ$ and (a) $\theta = 45^\circ$, (b) 90°, (c) 135°, and (d)-(f) $\theta = 90^\circ$ and (d) $\varphi = 0^\circ$, (e) 90°, (f) 180°. The linear color/gray scale gives the photoemission yield normalized to the maximum yields in (a)-(f).

problem, primarily since the spatial inhomogeneity of $\mathbf{E}_{tot}$ prevents the separation of Eq. (5) in spatial and temporal terms. However, as will be shown next, the accurate imaging of $\mathbf{E}_{tot}$ becomes possible since both the *quasi-static* and *slow-escape conditions* addressed earlier are met in the present study. Evaluation of the time integral in Eq. (2) at $\mathbf{k}_f = k_f\hat{\mathbf{n}}$ yields [34]

$$T_i(\mathbf{k}_f,\tau) = \frac{\sqrt{\pi}E_X}{i\omega_X}\hat{\mathbf{x}}^{lab}\cdot\int d^3\mathbf{r}\left[\nabla\Psi_i(\mathbf{r})\right]\Psi^{\tau *}_{\mathbf{k}_f}(\mathbf{r},t_z)e^{-i\omega_i t_z} \times \frac{1}{b^\tau_{\mathbf{k}_f}(\mathbf{r},t_z)}\exp\left\{-\left[\frac{\frac{\partial}{\partial t_z}\phi^\tau_{\mathbf{k}_f}(\mathbf{r},t_z)+\omega_X+\omega_i}{2b^\tau_{\mathbf{k}_f}(\mathbf{r},t_z)}\right]^2\right\}, \tag{8}$$

where

$$b^\tau_{\mathbf{k}_f}(\mathbf{r},t) = \sqrt{\frac{2\ln 2}{\tau_X^2}+\frac{i}{2}\frac{\partial^2}{\partial t^2}\phi^\tau_{\mathbf{k}_f}(\mathbf{r},t)}. \tag{9}$$

In spherical-wave approximation, the spatial integral in Eq. (8) can be approximated as [41, 42]

$$T_i(\mathbf{k}_f,\tau) \approx C_i\frac{\sqrt{2}\pi E_X R\, e^{-ik_f R - i\phi^\tau_{\mathbf{k}_f}(\hat{\mathbf{n}}R,\tilde{t}_z)}}{\omega_X k_f\; b^\tau_{\mathbf{k}_f}(\hat{\mathbf{n}}R,\tilde{t}_z)} \times \exp\left\{-\left[\frac{\frac{\partial}{\partial t_z}\phi^\tau_{\mathbf{k}_f}(\hat{\mathbf{n}}R,\tilde{t}_z)+\omega_X+\omega_i}{2b^\tau_{\mathbf{k}_f}(\hat{\mathbf{n}}R,\tilde{t}_z)}\right]^2\right\}, \tag{10}$$

where $\tilde{t}_z = R\cos\theta/c$ and

$$C_i = \int dr\left[\hat{\mathbf{x}}^{lab}\cdot\nabla\Psi_i(\hat{\mathbf{n}}r)\right]\cdot f[l(\hat{\mathbf{n}}r);\kappa)]. \tag{11}$$

Compliance with the *slow-escape* condition justifies the approximation

$$\frac{\partial}{\partial\tilde{t}_z}\phi^\tau_{\mathbf{k}_f}(\hat{\mathbf{n}}R,\tilde{t}_z) \approx -\mathcal{E}_f - \sqrt{2\mathcal{E}_f}\hat{\mathbf{n}}\int_{\tilde{t}_z}^{\infty}dt'\;\mathbf{E}_{tot}(\hat{\mathbf{n}}R,t'+\tau) = -\mathcal{E}_f - \sqrt{2\mathcal{E}_f}\hat{\mathbf{n}}\cdot\mathbf{A}_{tot}(\hat{\mathbf{n}}R,\tilde{t}_z+\tau), \tag{12}$$

where $\mathbf{A}_{tot}(\hat{\mathbf{n}}R,\tilde{t}_z+\tau)$ is the vector potential, whose quadratic (ponderomotive) term can be neglected at typical streaking-IR-field intensities [8]. Since $\mathbf{E}_{tot}$ can be assumed perpendicular to the nanoparticle surface (*quasi-static condition*), $\hat{\mathbf{n}}\cdot\mathbf{A}_{tot} = A_{tot}$, and thus

$$\frac{\partial}{\partial\tilde{t}_z}\phi^\tau_{\mathbf{k}_f}(\hat{\mathbf{n}}R,\tilde{t}_z) \approx -\mathcal{E}_f - \sqrt{2\mathcal{E}_f}A_{tot}(\hat{\mathbf{n}}R,\tilde{t}_z+\tau) \tag{13}$$

$$\frac{\partial^2}{\partial\tilde{t}_z^2}\phi^\tau_{\mathbf{k}_f}(\hat{\mathbf{n}}R,\tilde{t}_z) \approx \sqrt{2\mathcal{E}_f}\;E_{tot}(\hat{\mathbf{n}}R,\tilde{t}_z+\tau). \tag{14}$$

The photoemission probability can now be written integral-free as

$$P(\mathcal{E}_f)\big|_{\tau,\hat{\mathbf{n}}} \approx \sum_{i\in occ}\frac{\left|\pi C_i E_X R/\omega_X\right|^2\mathcal{E}_f^{-3/2}}{\sqrt{8\ln^2 2/\tau_X^4+\mathcal{E}_f E^2_{tot}(\hat{\mathbf{n}}R,\tilde{t}_z+\tau)}} \times \exp\left\{-\frac{\left[\mathcal{E}_f+\sqrt{2\mathcal{E}_f}A_{tot}(\hat{\mathbf{n}}R,\tilde{t}_z+\tau)-\omega_X-\omega_i\right]^2}{\sqrt{16\ln^2 2/\tau_X^4+2\mathcal{E}_f E^2_{tot}(\hat{\mathbf{n}}R,\tilde{t}_z+\tau)}}\right\}, \tag{15}$$

revealing that, despite being excited at different locations in the nanosphere, photoelectrons emerging at the surface in detection direction dominate the spectrum. This lays the foundation for retrieving plasmonically enhanced electric fields using streaked photoelectron spectra.

For the numerical application in this work, the XUV-pulse spectral range is limited by $2ln2/\tau_X = 4.56$ eV, such that the center of energy (CoE) can be approximated as [41]

$$\overline{\mathcal{E}_f}(\tau)\big|_{\hat{\mathbf{n}}} = \left.\frac{\int d\mathcal{E}_f\;\mathcal{E}_f P(\mathcal{E}_f)}{\int d\mathcal{E}_f\;P(\mathcal{E}_f)}\right|_{\tau,\hat{\mathbf{n}}} \approx \omega_X + V_0 + (3/5)\sigma_c - A_{tot}(\hat{\mathbf{n}}R,\tilde{t}_z+\tau)\sqrt{2\overline{\mathcal{E}_f}(\tau)}\;\Big|_{\hat{\mathbf{n}}}. \tag{16}$$

This enables the inversion of Eqs.(15) and (16) to an analytical expression for the net electric field at position $\hat{\mathbf{n}} = (\theta,\varphi)$ on the surface and time t [41],

$$E_{tot}(\hat{\mathbf{n}}R,t) = \frac{\partial}{\partial t}\left.\frac{\overline{\mathcal{E}_f}(t-R\cos\theta/c)-\omega_X-(3/5)\sigma_c-V_0}{\sqrt{2\overline{\mathcal{E}_f}(t-R\cos\theta/c)}}\right|_{\hat{\mathbf{n}}}. \tag{17}$$

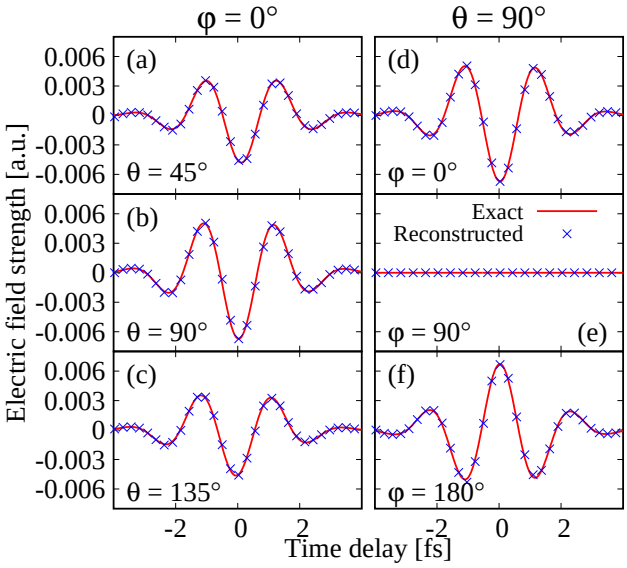

FIG. 3: (Color online) Time-resolved reconstruction of the net plasmonic field $E_{tot}(\hat{\mathbf{n}}R,t)$ at the surface of 50 nm radius Au spheres from the streaked photoelectron spectra in Fig. 2. Red solid lines show surface electric fields calculated within Mie theory. Positive values indicate fields pointing outward. Blue markers represent the electric-field reconstruction according to Eq. (17).

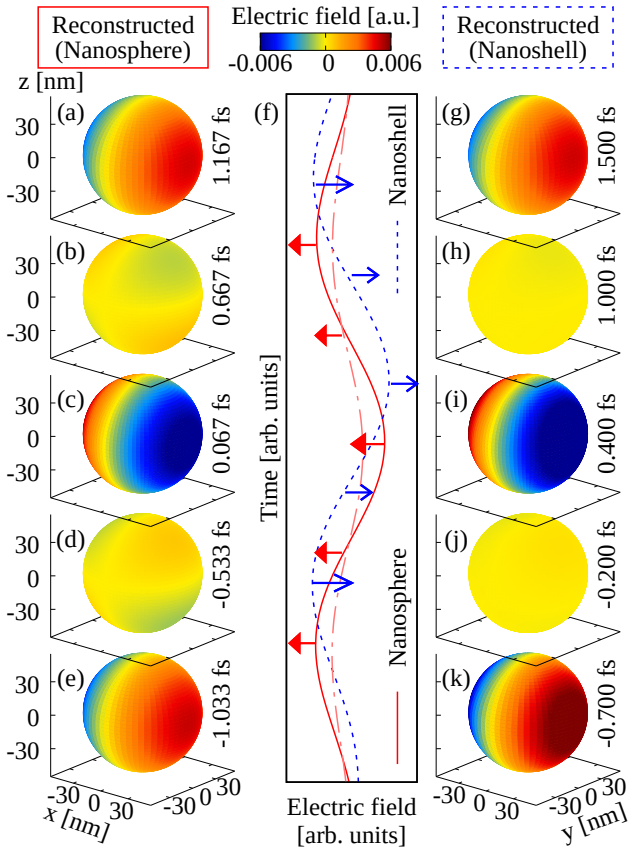

FIG. 4: (Color online) Spatiotemporal reconstruction of the net plasmonic field $E_{tot}(\hat{\mathbf{n}}R,t)$ at the surface of 50 nm radius Au (a)-(e) spheres and (g)-(k) shells with 45 nm inner radius at times indicated by arrows in (f). (f) $E_{tot}(\hat{\mathbf{n}}R,t)$ at the poles [$\hat{\mathbf{n}} = (90°, 0°)$] of the spheres (red solid) and shells (blue dashed line). Incident IR pulses with peak intensities of 10^{11} (thin red dot-dashed line) and 10^{10} W/cm^2 (not shown) are applied to spheres and shells, respectively.

This expression allows the spatiotemporal imaging of the surface plasmonic field with streaked photoemission.

Figure 3 shows the reconstruction of the time-dependent electric fields at the nanosphere surface from the streaked photoelectron spectra in Fig. 2. The time derivative in Eq. (17) is calculated using B-spline interpolation. The exact and retrieved electric fields are in excellent agreement. As observed in Fig. 2, (i) for given φ, maximum plasmonic enhancement occurs at the IR electric-field poles at $\theta = 90°$, and (ii) for given θ, the electric fields in forward ($\phi = 0°$) and backward ($\phi = 180°$) directions have opposite phases.

For the spatiotemporal reconstruction of $E_{tot}(\hat{\mathbf{n}}R,t)$ only angles θ for which the maximum photoemission yield is no less than half of the maximum yield obtained at $\theta = 90°$ are included. While not mandatory, this restriction improves the accuracy of the field retrieval since the photoemission yield decreases with θ proportional to $\cos^2(\theta - 90°)$. We assume a uniformly spaced angular grid with $(n_\theta \times n_\varphi)$ points for $\theta \in [45°, 135°]$ and $[0°, 360°)$. Figure 4(a)-(e) show the spatiotemporal profiles of the incident pulse and the reconstructed plasmonically enhanced electric field at the nanosphere surface at the times t indicated in Fig. 4(f). The field is provided on an $(n_\theta \times n_\varphi) = (6 \times 8)$ angular grid and B-spline interpolated over the entire $\theta \in [0°, 180°]$ angular range. Both, the temporal oscillation and spatial propagation are observed in the reconstructed fields. A comparative animation of the spatiotemporally-resolved exact and reconstructed electric field at the surface of the nanosphere is found in Supplementary Material [41].

As a second numerical example, we show reconstructed electric fields at the surface of Au nanoshells in Fig. 4(g)-(k) [43, 44]. Since the plasmon resonance of the shells is near the streaking-pulse wavelength, we reduced the IR-pulse intensity to 10^{10} W/cm^2, in order to yield comparable peak intensities of $E_{tot}(\hat{\mathbf{n}}R,t)$ for spheres and shells. For both spheres and shells Mie-theory-calculated and reconstructed plasmonic fields are in excellent agreeement [41].

The plasmonic-field-retrieval accuracy for Au nanospheres is quantified in Fig. 5 in terms of the average error (including all times and the entire nanoparticle surface)

$$Err = \frac{\int d\hat{\mathbf{n}} \int dt \; \left| E_{tot}(\hat{\mathbf{n}}R,t) - E_{exa}(\hat{\mathbf{n}}R,t) \right|}{\max\left\{ |E_{exa}(\hat{\mathbf{n}}R,t)| \right\} \; \int d\hat{\mathbf{n}} \int dt} \qquad (18)$$

as a function of the angular grid size. the error does not exceed 1.5%, and quickly converges in n_θ and n_φ.

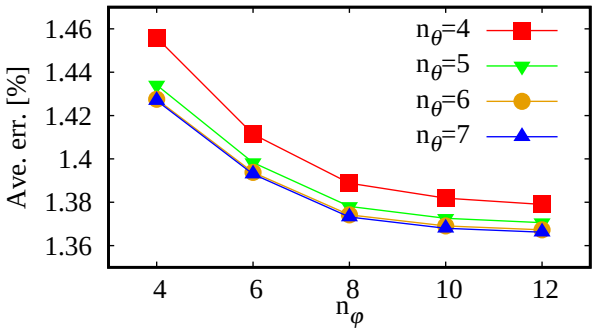

FIG. 5: (Color online) Average field-reconstruction error for different numbers of grid points n_θ and n_φ.

The 1.36% residual (systematic) error cannot be reduced by further increasing the number of angular grid points, due to the physical and mathematical approximations introduced in our reconstruction method [41].

In summary, based on a quantum-mechanical model, we show that under *quasi-static* and *slow-escape conditions* the spatiotemporally-resolved plasmonically enhanced electric field at the surface of metallic nanospheres and nanoshells can be reconstructed with high accuracy from streaked photoelectron spectra based on a simple analytical expression. This suggests the usage of streaked photoelectron spectroscopy to image spatiotemporally-resolved electric fields at nanoparticles and nanostructured surfaces.

This work was supported in part by the Air Force Office of Scientific Research award no. FA9550-17-1-0369 (Recollision physics at the nanoscale), NSF grant no. PHY 1464417 (Theory for photoemission from surfaces), and the Chemical Sciences, Geosciences, and Biosciences Division, Office of Basic Energy Sciences, Office of Science, U.S. DOE (Attosecond interferometry and photoemission from atoms in spatially varying external fields).

[1] B. H. Bransden and C. J. Joachain, *Physics of atoms and molecules* (Englewood Cliffs, NJ, Prentice–Hall, 2003).
[2] K. T. Kim, D. M. Villeneuve, and P. B. Corkum, Nat. Photonics **8**, 187 (2014).
[3] F. Krausz and M. I. Stockman, Nat. Photonics **8**, 205 (2014).
[4] S. R. Leone *et al.*, Nat. Photonics **8**, 162 (2014).
[5] M. Lucchini, A. Ludwig, L. Kasmi, L. Gallmann, and U. Keller, Opt. Express **23**, 8867 (2015).
[6] C. Chen *et al.*, **114**, E5300 (2017).
[7] M. Schultze *et al.*, Science **328**, 1658 (2010).
[8] U. Thumm, Q. Liao, E. M. Bothschafter, F. Süßmann, M. F. Kling, and R. Kienberger, *Fundamentals of photonics and physics* (Wiley, 2015).
[9] S. Neppl, R. Ernstorfer, E. M. Bothschafter, A. L. Cavalieri, D. Menzel, J. V. Barth, F. Krausz, R. Kienberger, and P. Feulner, Phys. Rev. Lett. **109**, 087401 (2012).
[10] Q. Liao and U. Thumm, Phys. Rev. Lett. **112**, 023602 (2014).
[11] S. Neppl *et al.*, Nature **517**, 342 (2015).
[12] Q. Liao and U. Thumm, Phys. Rev. A **92**, 031401 (2015).
[13] L. Seiffert *et al.*, Nat. Physics **13**, 766 (2017).
[14] F. Siek *et al.*, Science **357**, 1274 (2017).
[15] R. Locher, L. Castiglioni, M. Lucchini, M. Greif, L. Gallmann, J. Osterwalder, M. Hengsberger, and U. Keller, Optica **2**, 405 (2015).
[16] Z. Tao, C. Chen, T. Szilvási, M. Keller, M. Mavrikakis, H. Kapteyn, and M. Murnane, Science **353**, 62 (2016).
[17] V. Loriot *et al.*, J. Opt. **19**, 114003 (2017).
[18] A. L. Cavalieri *et al.*, Nature **449**, 1029 (2007).
[19] M. I. Stockman, Phys. Today **64**, 39 (2011).
[20] M. I. Stockman, M. Kling, U. Kleineberg, and F. Krausz, Nat. Photonics **1**, 539 (2007).
[21] B. Barwick, D. J. Flannigan, and A. H. Zewail, Nature **462**, 902 (2009).
[22] J. Lin, N. Weber, A. Wirth, S. H. Chew, M. Escher, M. Merkel, M. F. Kling, M. I. Stockman, F. Krausz, and U. Kleineberg, J. Physics: Condens. Matter **21**, 314005 (2009).
[23] C. Lemke *et al.*, Nano Letters **13**, 1053 (2013).
[24] B. Förg *et al.*, Nat. Commun. **7**, 11717 (2016).
[25] M. I. Stockman, Opt. Express **19**, 22029 (2011).
[26] J. Feist, M. T. H. Reid, and M. F. Kling, Phys. Rev. A **87**, 033816 (2013).
[27] W. Zhu, R. Esteban, A. G. Borisov, J. J. Baumberg, P. Nordlander, H. J. Lezec, J. Aizpurua, and K. B. Crozier, Nat. Commun. **7**, 186 (2016).
[28] X. Zhang, Y. L. Chen, R.-S. Liu, and D. P. Tsai, Rep. Prog. Phys. **76**, 046401 (2013).
[29] M. T. Sheldon, J. van de Groep, A. M. Brown, A. Polman, and H. A. Atwater, Science **346**, 828 (2014).
[30] E. Yasun, H. Kang, H. Erdal, S. Cansiz, I. Ocsoy, Y.-F. Huang, and W. Tan, Interface Focus **3** (2013), 10.1098/rsfs.2013.0006.
[31] W. Chen *et al.*, Nanomedicine **9**, 1209 (2014).
[32] M. Müller, V. Kravtsov, A. Paarmann, M. B. Raschke, and R. Ernstorfer, ACS Photonics **3**, 611 (2016).
[33] J. Li, E. Saydanzad, and U. Thumm, Phys. Rev. A **94**, 051401 (2016).
[34] J. Li, E. Saydanzad, and U. Thumm, Phys. Rev. A **95**, 043423 (2017).
[35] E. Saydanzad, J. Li, and U. Thumm, Phys. Rev. A **95**, 053406 (2017).
[36] G. Mie, Ann. Phys. **330**, 377 (1908).
[37] J. Stratton, *Electromagnetic theory*, Vol. 33 (Wiley, 2007).
[38] F. Süßmann and M. F. Kling, Phys. Rev. B **84**, 121406 (2011).
[39] F. Kelkensberg, A. F. Koenderink, and M. J. J. Vrakking, New J. Phys. **14**, 093034 (2012).
[40] S. Tanuma, C. J. Powell, and D. R. Penn, Surface and Interface Analysis **43**, 689 (2011).
[41] The supplementary material at *[URL]* provides mathematical derivations and includes an animation of the Mie-theory-calculated and reconstructed electric near-field distributions for Au nanospheres and nanoshells.

[42] E. Merzbacher, *Quantum Mechanics*, 3rd ed. (Wiley, 1998) p. 262.
[43] Y. Jin, Acc. Chem. Res. **47**, 138 (2013).
[44] Y. Sun, B. Mayers, and Y. Xia, Adv. Mater. **15**, 641 (2003).